Combined Effects of Flow/Spray Interactions and EGR on Combustion

Variability for a Stratified DISI Engine

Wei Zeng[a], Magnus Sjöberg[a], David Reuss[a,b]

a Sandia National Laboratories, MS 9053, PO Box 969, Livermore, CA 94551-0969, USA

b University of Michigan, 1231 Beal Ave., Ann Arbor, MI, 48109, USA

Fax: +1 925 294 1004

Email address: wzeng@sandia.gov (W. Zeng)

Colloquium: IC ENGINE AND GAS TURBINE COMBUSTION

Method 1

Main Text	3422
Figure 1 with caption	174
Figure 2 with caption	104
Figure 3 with caption	213
Figure 4 with caption	148
Figure 5 with caption	377
Figure 6 with caption	136
Figure 7 with caption	157
Figure 8 with caption	279
Figure 9 with caption	152
Figure 10 with caption	152
Table 1	167
Table 2	61
Equation 1	23
Reference	227
Total words	5793

Combined Effects of Flow/Spray Interactions and EGR on Combustion Variability for a Stratified DISI Engine

Wei Zeng[a], Magnus Sjöberg[a], David Reuss[a,b]

a Sandia National Laboratories, MS 9053, PO Box 969, Livermore, CA 94551-0969, USA

b University of Michigan, 1231 Beal Ave., Ann Arbor, MI, 48109, USA

Abstract

This study investigates combustion variability for a stratified-charge direct-injection spark-ignited (DISI) engine, operated with near-TDC injection of E70 fuel and a spark timing that occurs during the early part of the fuel injection. Using EGR, low engine-out NO_x can be achieved, but at the expense of increased combustion variability at higher engine speeds. Initial motored tests at different speeds reveal that the in-cylinder gas flow becomes sufficiently strong at 2000 rpm to cause significant cycle-to-cycle variations of the spray penetration. Hence, the fired tests focus on operation at 2000 rpm with N_2 dilution ($[O_2]$ =19% and 21%) to simulate EGR. In-cylinder flow, spray, and early-flame measurements are correlated to reveal their effect on the combustion variability.

Results reveal two types of flow/spray-interactions that predict the likelihood of a partial burn. 1) Proper flow direction before injection with a more collapsed spray leads to high kinetic energy of the flow during injection, thus generating a rapid early burn, which ensures complete combustion, regardless of the EGR level. 2) Improper flow direction and less collapsed spray generate low flow energy during the early phase of combustion. For this second type of flow/spray-interaction, application of EGR results in a partial-burn frequency of 30%, whereas without EGR, early combustion is shown to be insensitive to flow variations. Flame-probability maps illustrate that the partial-burn cycles for operation with EGR have a weak flame development in that the flame does not develop uniformly and reliably from the spark plug. Without EGR, the flame development is more repeatable regardless of the type of flow/spray-interaction, at the expense of higher NO_x emissions.

Key words: Stratified DISI Engine, Combustion variability, Flow/Spray Interactions, EGR, Optical diagnostics

1. Introduction

High efficiency can be achieved in spark-ignited automotive engines using un-throttled stratified-charge combustion for load control. However, practical implementation is inhibited by the need for lean-NO_x and particulate aftertreatment [1, 2]. Recent studies by the authors have demonstrated that legislated levels of engine-out NO_x and soot abatement can be achieved using EGR combined with ethanol-gasoline blends, which enable later injection and spray-head ignition compared to pure gasoline. However, the in-cylinder emission control is limited to a small speed and load range due cyclic variability [3, 4]. Further research has been undertaken to identify the causes of the combustion variability with the goal of expanding the operating range. Testing at 1000 and 2000 rpm led to two hypotheses; a) The spray-guided stratified-charge combustion rate is primarily controlled by the mixing rates and turbulence level associated with fuel injection, but b) the in-cylinder flow field, generated by the intake and compression strokes, stochastically disturbs the mixing and flow associated with the fuel jets, thereby causing cycle-to-cycle variations of the combustion [5]. Particle image velocimetry (PIV), flame and liquid-spray measurements of non-fired operation support these hypotheses [6]. In this study, these in-cylinder optical diagnostics are instead applied to fired operations for correlation with the combustion variability. Here, tests are performed at 2000 rpm with and without N_2 dilution, and apparent differences in flow and combustion variability are observed.

2. Experimental setup and methodology

2.1 Single cylinder engine

Testing was performed in a single-cylinder four-valve pent-roof DISI engine, operated with late injection for stratified-charge combustion. In a spray-guided configuration, the injector was located near the cylinder axis and oriented with two of the eight jets straddling the ground electrode of the spark plug. The engine was operated in an all-metal configuration for continuously fired performance testing or in a geometrically identical optical configuration as shown in Fig.1. For optical access the Bowditch piston was equipped with a plano-concave (R=25 mm) quartz-window to create a flat-bottom piston bowl with a large viewing angle. Also, a flat quartz-window was located in the end of the pent-roof section closest to the injector to enable observation along the axis of the pent-roof. E70 fuel was used, blended from 70% ethanol and 30% research-grade gasoline with (R+M)/2 =87 [5]. All tests in this study were conducted with one intake valve deactivated to increase in-cylinder swirl and tumble levels, which generally provide more robust stratified operation. For fired engine operation, N_2 dilution was used to lower the intake mole fraction of oxygen $[O_2]$ to simulate EGR. In-cylinder pressure was acquired with 0.1° crank-angle (CA) resolution for 500 consecutively fired cycles during all-metal engine operations. The apparent heat-release rate (AHRR) was computed from the in-cylinder pressure using a constant ratio of specific heats (γ)

following Ref. [7]. NO emissions were measured using a Horiba MEXA-584L emission analyzer. Engine specifications and operating conditions are given in Table 1. Tests 1-3 are all-metal performance operations. A complete description of the hardware and analysis is provided in Ref. [5].

2.2 Optical diagnostics

High-speed planar PIV, combustion luminosity, and spray images were acquired for Tests 4&5 to measure the in-cylinder gas flow, fuel injection, and combustion processes. A 25% duty cycle Fire2-Skip6 sequence was used to reduce the thermal load. In-cylinder pressure and optical data were acquired during the second fired cycle to ensure proper temperature and composition of the residual gases. Image data were limited to 70 cycles per test, due to obscuration by soot deposits on the windows.

The PIV images were recorded by a CMOS camera (Phantom v710) through the pent-roof window to provide instantaneous two-dimensional (2D) view of the tumble plane. Camera-views and laser sheet location are shown in Fig.1. The v710-camera was angled downward to view into the bowl creating a systematic 8% error in the vertical velocity that was uncorrected, but does not affect the comparisons or conclusions in this study. The silicone oil droplets, which have mean diameters of 1 μm, were illuminated by a 2 mm thick 532 nm laser sheet, which was directed through the piston window, normal to the ridge of the pent-roof, and passing between the spark plug and the injector. The dual-cavity laser produced two 4 mJ pulses with an interval of 10 μs (Δt) at every 2.0°CA (6kHz). The relatively thick laser sheet is the result of the plano-concave piston-bowl window. The 1200 x 440 pixel PIV image pairs (one pair per 2°CA) were recorded at 12 kHz using frame straddling. The 0.75 magnification produced a 47×17 mm field of view with 0.98 mm^2 square (32×32 pixel) PIV interrogation spots on a 0.5 mm^2 grid. Thus there is an in-plane spatial resolution of 1 mm and a velocity dynamic range of 0.58 – 31.3 m/s. The valid-vector rate was greater than 80%. Details of the PIV measurement hardware, post-processing, and uncertainty analysis are detailed in Ref. [6].

Simultaneously with the PIV and spray measurements through the side window (tests 4 & 5), flame and spray images were acquired every 1°CA (12 kHz) through the piston-bowl window by another CMOS camera (Phantom v7.1), using 384x384 pixel resolution. A 532±10 nm notch filter was installed to reject scattered laser-light. The optical setup is also detailed in Ref. [6]. The spray was illuminated using a high-intensity blue LED with a 2-μs-pulse duration via the pent-roof end-window.

Separate spray images were acquired in tests 6 & 7 to measure the effect of the in-cylinder gas flow on liquid spray variability. Sprays were imaged through the piston-bowl window with a color CMOS camera (Phantom v611) operated at a

20 kHz frame rate and illuminated via the pent-roof end-window using a high-intensity green LED with a 4-µs-pulse duration. Data were acquired for 200 non-fired cycles at 333 and 2000 rpm. These engine speeds were chosen to compare relatively weak and strong in-cylinder flows.

3. Results and discussion

3.1 Engine combustion performance

All-metal experiments (tests 1-3 in Table 1) for $[O_2]$ sweep at 2000 rpm were carried out to quantify the effect of EGR on combustion and exhaust emissions, and establish the conditions for optical experiments in tests 4 & 5. A head-ignition strategy (ignite the leading edge of spray) was applied to achieve closely coupled injection and combustion, which can provide ultra-low NO emissions. Here the soot level is relatively high (FSN ≈ 0.52-0.58). The combined effects of fuel type and ignition strategies on soot emissions are discussed in Ref. [8] but are outside the scope of this discussion. Injection and spark timings were adjusted to achieve CA50 ≈ 7-8°CA. Figure 2 shows that NO emissions decrease strongly for lower $[O_2]$, at the expense of elevated combustion variability and decreased combustion efficiency. The importance of realizing both low NO_x and stable combustion motivates an investigation of the cause of the observed combustion variability. As mentioned in the introduction, at 2000 rpm the in-cylinder flow field generated by the intake and compression strokes becomes sufficiently strong to significantly contribute to cycle-to-cycle variations of the mixing rates and turbulence level associated with the spray. Generally, a reduction of $[O_2]$ weakens both premixed and non-premixed flames, with an associated reduction of both the flame speed and the strain rate where extinction occurs. With respect to Fig. 2, it is then hypothesized that for low $[O_2]$, the flame weakens sufficiently to the point of being susceptible to variations of flow/spray interactions, occasionally degrading the combustion efficiency, thereby elevating the variability of $IMEP_g$ (indicated mean effective pressure-gross).

To examine the validity of this hypothesis, optical diagnostics were carried out for fired operations with $[O_2] = 21\%$ and 19% (tests 4&5). Flow variations before and during injection, and their effects on spray development and flame propagation are studied. For test 5, 7 partial-burn cycles are observed out of the total 140 cycles (conducted twice.), while all 70 cycles from test 4 burn well. Here, partial burns are defined to have a final mass fraction burned (FMFB) below 80%.

3.2 Variations of liquid spray

Spray-Mie images (tests 6&7) for 2000 rpm are shown in Fig. 3a to reveal the effect of in-cylinder flow variability on liquid spray. The images are shown at 0.20 ms after start of injection ($ASOI_a$), corresponding to 20% of the injection duration. The difference in the location of the sprays relative to the overlay for both examples indicates that the liquid jets appear to rotate

in unison from cycle to cycle. Variations in individual plume spread and jet trajectory are also observed. In addition, a significant variation of radial penetration (defined in Fig. 3b) is observed for the 1:00- and 11:00-jets. The threshold is defined according to the SAE Standard-J2715. To quantify this, Fig. 3b presents average penetration of the 1:00-jet and its coefficient of variation (COV) for 333 and 2000 rpm. The disparate engine speeds (and thus large differences of the flow variations) were chosen to show this effect more clearly. A sudden increase in the COV is found at 0.2 ms $ASOI_a$ for 2000 rpm, while the magnitude of COV is constant for 333 rpm. This demonstrates that the in-cylinder flow becomes sufficiently strong to impact the spray structure at 2000 rpm. These observations of spray variations motivate simultaneous measurement of flow and spray structures, as discussed below.

3.3 Flow/spray interaction and its effect on combustion variability

Figures 4 and 5 demonstrate the flow/spray interactions for test 5. The PIV measurement focused on the tumble plane between the spark plug and the injector tip. The laser sheet illuminated both liquid spray and PIV-seeds during the injection, hence flow and spray structures were imaged simultaneously. The spatially averaged kinetic energy (KE) of the gas flow was calculated to represent the flow energy for analysis (excluding vectors computed in the spray), as defined in Eqn. 1. The left-half of each vector field is not shown and is not included in the KE-calculation due to the obscuration by soot deposits. *u* and *v* are the x- and y-velocity components of vectors with indices *i* and *j* on a 2D grid, *m* × *n* in size. *k* represents the number of the cycle. To quantify the flow direction, spatial average of all vectors in the dashed rectangle indicated in Fig. 5 is calculated and the direction of this averaged vector is defined as flow angle. Along with the flow angle, the included angle of the spray is also quantified based on the SAE-J2715 standard.

$$KE_k = \frac{1}{n \times m} \sum_i^n \sum_j^m (u_{i,j,k}^2 + v_{i,j,k}^2) \quad (1)$$

The COV curve in Fig. 4 shows that cycle-to-cycle variations of the flow remain high for CAs after SOI_a. Three selected cycles in Figs. 4 & 5 exemplify the combined effects of flow and spray. Figure 5 shows different combinations of flow/spray-structures and flow energy. In example 1, a high KE during injection corresponds to a small spray angle and large flow angle. On the contrary, examples 2 and 3 show that low flow energy corresponds to a large spray angle and small flow angle. These observations suggest that different types of the flow/spray interactions exist.

The observed spray angles in examples 1 & 3 are smaller than the nominal included spray angle of the injector (60°), indicating a certain degree of spray collapse [9]. Meanwhile, the spray angle varies significantly from cycle to cycle, in agreement with the spray variations in Fig. 3. However, both the role of the flow for the spray collapse, and the impact of the

collapse on subsequent gas-flow entrainment remain unclear. Further studies are required for a better understanding of these cycle-to-cycle variations.

In the following, statistical analysis is used to correlate the flow and spray structures with both the KE of the flow during injection and with the partial-burn cycles using the spray angle at -17°CA against the flow angle at -21°CA, as identified in Fig.6. There are two important observations. First, cycles characterized by small spray angles with large flow angles (before injection) exhibit high KE and burn well, as indicated by the top 15% KE cycles. Second, all partial-burn cycles are heavily biased toward large spray angles (>52.5°) and small flow direction angles (<100°). These observations reveal that the flow energy during injection correlates to some degree with the combined effects of the flow and spray angles. It is then possible that a proper flow direction before injection combined with a more collapsed spray results in a strong interaction between spray and flow to generate high kinetic energy of the flow during injection. These factors are assumed to result in favorable fuel/air-mixing and turbulence levels during the early burn, which leads to a high burn rate and ensures a more complete combustion event.

3.4 Correlations between flow energy and combustion performance

To further understand the flow-field effects on combustion variability, Figs. 7a & 7b plot $IMEP_g$ against KE of gas flow for the 140 individual cycles from test 5 ($[O_2]$ =19%). Figure 7a shows no apparent trend, possibly illustrating that there is no direct correlation between the combustion performance and the pre-injection tumble flow, as measured in this PIV plane. However, Fig.7b plots KE during injection and shows that all cycles with relatively high KE (>63 m^2/s^2) have normal $IMEP_g$ values (around 260 kPa) and are considered to burn well. All partial-burn cycles (< 222 kPa) exhibit relatively low KE. This suggests that low flow energy during injection is a predictor of increased likelihood for partial-burn cycles. Still, most cycles with low KE burn well. Given the 3-D nature of both flow and combustion, it is natural that flow variations in the measurement plane are not the only cause of cycle-to-cycle combustion variability.

Based on the observations for the spray and flow structures (Figs. 5 & 6) and the correlation between the flow energy during injection and the $IMEP_g$ (Fig. 7), the flow/spray interactions can be classified into two important types, as stated in Table 2. The ranges of KE, flow and spray angles for the strong-flow cycles are determined from the top-15% KE cycles shown in Fig. 6, while those for the weak-flow cycles are determined from the partial-burn cycles. All strong-flow cycles burn well, while 30% of all weak flow cycles develop into partial burns.

To understand how the flow affects the combustion rate, AHRR data are compared for normal (FMFB>80%) and partial-burn cycles using conditional analysis based on the flow and spray conditions shown in Table 2. Figure 8a plots the AHRR curves

for the three examples. Example 1 (well burning cycle with high KE) exhibits a high burn rate during the early burn (from ST to -5°CA). It is speculated that high flow energy during injection causes favorable fuel/air-mixing and turbulence levels, thus leading to fast flame kernel formation and flame propagation. Examples 2 & 3 both exhibit relatively slow early burn phases, which is consistent with the relatively low flow energy during injection. However, example 2 burns completely, whereas example 3 develops into a partial burn. These results are similar to observations by Peterson *et al.* [10] in that having a slow early burn with low flow energy is necessary but not sufficient to predict partial burns.

Figure 8b plots in detail the early AHRR for the top-15% KE cycles and the 7 partial-burns cycles which have small KE. Figure 8b agrees with Figs. 7 and 8a and indicates that, statistically, high KE corresponds to higher-than-average early AHRR, ensuring a well burning cycle. In contrast, all partial-burn cycles have low early AHRR and a delayed transition into the main combustion, consistent with a small KE during injection. Overall, these observations show the importance of the flow during injection for the early stages of stratified combustion using head ignition.

Figure 8c presents the AHRR curves for operation without EGR in test 4 ($[O_2]$ =21%). Using the thresholds in Table 2, 10 strong-flow cycles and 10 weak-flow cycles are identified among the 70 cycles. However, in this case, the flow strength is not a predictor of the magnitude of the early AHRR, and all cycles eventually burn to completion. Apparently, the higher $[O_2]$ level for this condition makes the early combustion insensitive to flow variations.

3.5 Effects of flow/Spray interactions and EGR on early-flame variability

This section describes the use of flame imaging to quantify the cyclic variability of the early-flame growth as impacted by flow strength and EGR. Figure 9 shows two cycles indicating that the flame growth is faster with higher $[O_2]$. Hence, to compare the two tests for timings with similar flame size and AHRR, flame images at -13°CA for test 4 and at -9°CA for test 5 are used for Fig.10.

Thresholding is applied to the flame images to define the extent and location of the flame in each cycle and to create ensemble-sampled two-dimensional probability maps, as per Ref. [11]. Conditionally sampled flame-probability maps are shown in Fig. 10 for cycles with strong flow, weak flow, and weak flow with partial burns. Here, flow strength is defined as for Fig. 8. For strong-flow cycles (Figs. 10a & 10c), large, comparatively radially symmetric, and contiguous high-probability regions are observed and centered just to the left of the ground strap for both $[O_2]$ levels. The equivalence of Figs.10a & 10c indicates that the early flame growth is not hampered by a reduction of $[O_2]$ when the flow is sufficiently strong. For the cycles with $[O_2]$ = 21% and weak-flow shown in Fig. 10b, it is observed that statistically the flame still develops circularly despite the weak flow. However, for the lower $[O_2]$ in Fig. 10d, there is a clear tendency for the weak-

flow cycles to develop reliably only in a small region to the left of the spark plug. Note that Fig. 10d is based on all 25 weak-flow cycles, including 7 that are partial burns. Figure 10e samples the 7 partial burns alone. Here, it becomes obvious that the probability of a flame is restricted to a very small region on the left side of the spark plug. The observations in Fig. 10 reveal that the effects of flow/spray-interactions on flame propagation become stronger for low-NO_x operation with EGR as a result of a weaker early flame kernel and less robust flame structure at lower $[O_2]$. This occasionally degrades the consumption of the fuel/air mixture, causing partial burn cycles, supporting the hypothesis in section 3.1.

Comparisons among Figs. 10c-e and further inspection of the pressure-based HRR curves in Fig. 8a reveal that most of the weak-flow cycles have sufficient combustion and that the most probable flame develops in the same direction as the well burning cycles, independent of flow strength. Therefore, it can be surmised that the flow strength (in this measurement plane) is not the cause of the slow growth but an indicator of another change. Since increased O_2 (in an otherwise statistically equivalent fuel concentration and flow) ensures complete combustion, it indicates that partial burns are due to changes in the transition from the flame kernel to a fully developed flame. Possibilities include flow-induced flame stretch or overmixing in the tail of the spray due to the delayed kernel-to-turbulent-flame transition.

4. Conclusions

For engine operation at 2000 rpm, the in-cylinder air flow generated by the intake and compression strokes is sufficiently strong to cause cycle-to-cycle variability of stratified combustion when EGR is applied to achieve low NO_x emissions. PIV, spray- and flame-imaging are used to elucidate the in-cylinder mechanisms leading to undesirable partial-burn cycles. Analysis reveals two types of flow/spray-interactions, which can be used to predict likelihood for a particular cycle to develop into a partial burn; 1) a proper flow direction before injection with a more collapsed spray causes strong flow/spray interactions, ensuring high kinetic energy of the flow during injection. This typically leads to a fast early burn, which ensures complete combustion, even for operation with EGR. 2) An improper flow direction and a less collapsed spray generate low flow energy during injection. For this type of flow/spray-interaction, 30% of the cycles exhibit weak early heat release and develop into partial burns when EGR is applied. Hence, having weak gas flow near the fuel spray during injection is thought to be one mechanism that contributes to the appearance of partial-burn cycles.

Flame-probability maps reveal that the partial-burn cycles for operation with EGR have a weak and variable flame development. Without EGR, the flame development away from the spark plug is more repeatable regardless of the type of flow/spray-interaction, at the expense of higher NO_x emissions.

9

Reference

1. H. Ando, C. Arcoumanis, *Flow and Combustion in Reciprocating Engines*, Springer-Verlag, Berlin Heidelberg, 2008, p. 137, Chapter.3.

2. M.C. Drake, D.C. Haworth, *Proc. Combust. Inst.* 31 (2007) 99-124.

3. M. Sjöberg, D.L. Reuss, *SAE Int. J. Fuels Lubr.* 5 (2012) 1096-1113.

4. M. Sjöberg, D.L. Reuss, *Proc. Combust. Inst.* 34 (2013) 2933-2940.

5. M. Sjöberg, W. Zeng, D. L. Reuss, submitted to *SAE congress 2014*, paper offer #14PFL-468.

6. W. Zeng, M. Sjöberg, D. L. Reuss, submitted to *SAE Congress 2014*, paper offer #14PFL-469.

7. J.B. Heywood, *Internal Combustion Engine Fundamentals*, McGraw-Hill, New York, 1988.

8. M. Sjöberg, W. Zeng, D. L. Reuss, *2013 Hyundai-Kia International Powertrain Conference*.

9. W. Zeng, M. Xu, G. Zhang, Y. Zhang, D.J. Cleary, *Fuel* 95 (2012) 287-297.

10. B. Peterson, D.L. Reuss, V. Sick, *Proc. Combust. Inst.* 33 (2011) 3089–3096.

11. W. Zeng, C.A. Idicheria, T.D. Fansler, M.C. Drake, *SAE Technical Paper* 2011-01-1281, 2011.

Table 1

Engine specifications and operating conditions

Bore/Stroke/ Displacement (liter)	86.0 / 95.1 / 0.55
CR/Swirl/Tumble Ratios	12:1 / 2.7 / 0.6
Ave Ign Energy / Dur	106 mJ / 1.0 ms
Fuel injector	Bosch 8-hole w/60° included angle
Injection-duration/Fuel-mass	0.925 ms /12.6 mg
Intake / coolant temperatures	25-28°C / 60°C
Injection Pressure/Fuel	17 MPa / E70
Intake pressure (abs.)	95 kPa

Test Configuration	*[O_2]*	*SOIe/SOIa/ST*(°CA*	*RPM*
1.All-metal	21%	-20/-16/-14	2000
2.All-metal	20%	-22/-18/-16	2000
3.All-metal	19%	-25/-21/-19	2000
4.PIV/flame/spray	21%	-25/-21/-19	2000
5.PIV/flame/spray	19%	-25/-21/-19	2000
6.Spray alone	21%	-22.8/-18.6/~	2000
7.Spray alone	21%	-22.8/-22.2/~	333

*SOIe = start of injection (electrical signal). SOIa = start of injection (appearance of liquid). ST = start of spark discharge.

Table 2

Classification of flow/spray interaction

	KE*	Flow angle	Spray angle
Strong flow	>86 m^2/s^2	>100°	<52.5°
Weak flow	<63 m^2/s^2	<100°	>52.5°

*KE only reflects the flow during injection.
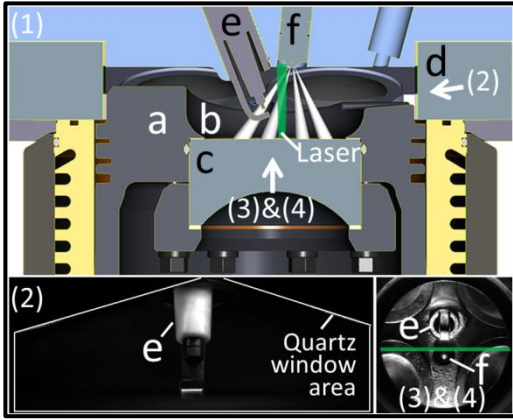
Fig.1. (1) single-cylinder optical engine with (a)-piston, (b)-piston bowl, (c)-piston-bowl window, (d)-pent-roof window, (e)-spark plug, and (f)-fuel injector, (2) camera view for PIV, (3) camera view for flame, (4) camera view for liquid-spray
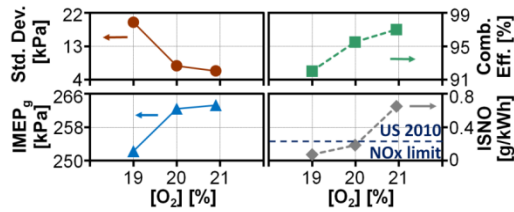

Fig.2. Combustion efficiency, $IMEP_g$, standard deviation of $IMEP_g$ and NO emission for all-metal engine operation obtained by sweeping intake $[O_2]$ at 2000 rpm.
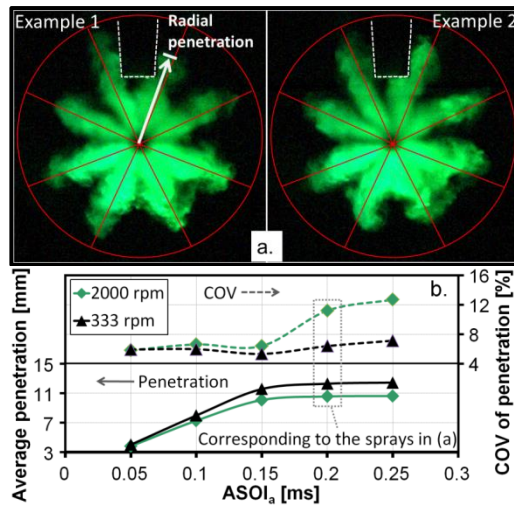

Fig.3. (a) two individual spray images recorded 0.20 ms $ASOI_a$ at 2000 rpm, test 6. The overlay is for reference and indicates the expected jet trajectories. (b) Averaged radial penetration of 1:00-jet and its COV for both 333 (test 7) and 2000 rpm (test 6).

12
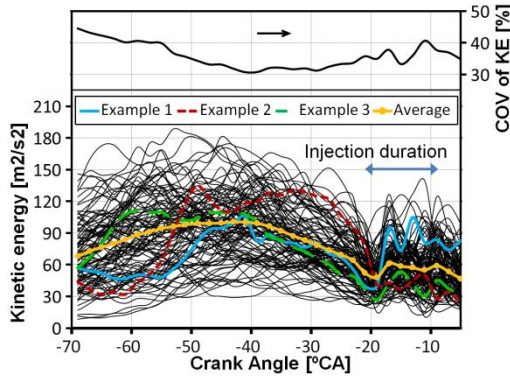
Fig.4. Spatially-averaged kinetic-energy (KE) for 140 cycles and its COV at 2000 rpm with [O$_2$] =19%, test 5.
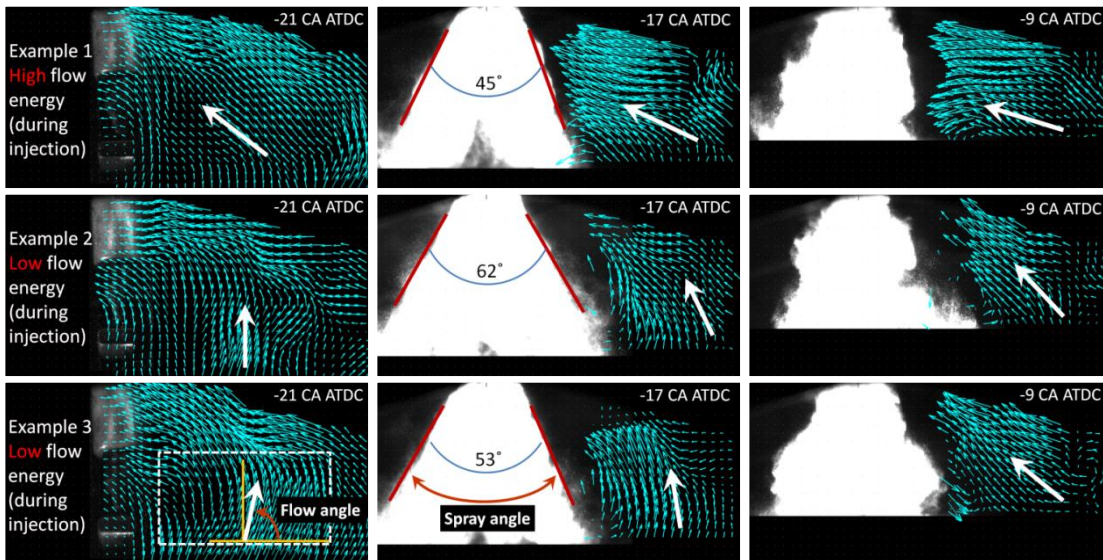
Fig.5. Flow field evolutions with spray structures for the three specially selected cycles indicated in Fig.4.
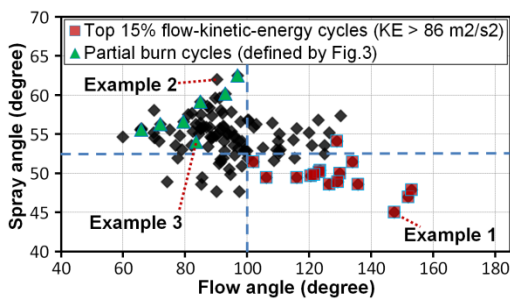
Fig.6. Spray and flow angles for 140 individual cycles at 2000 rpm operation with [O$_2$] = 19% (test 5) and kinetic energy of the flow during injection and with partial-burn cycles.

13
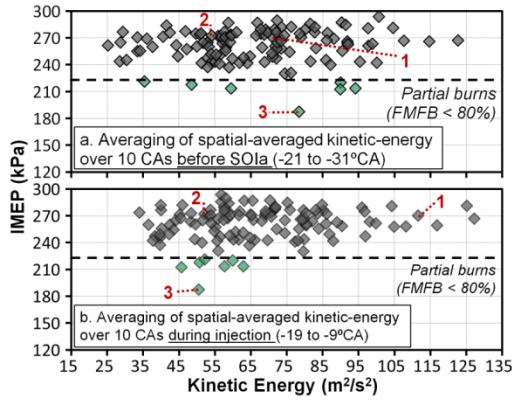
Fig.7. IMEP$_g$ against spatially averaged KE of gas flow, averaged over 10°CA before SOI$_a$ (a) and during injection (b), test 5.
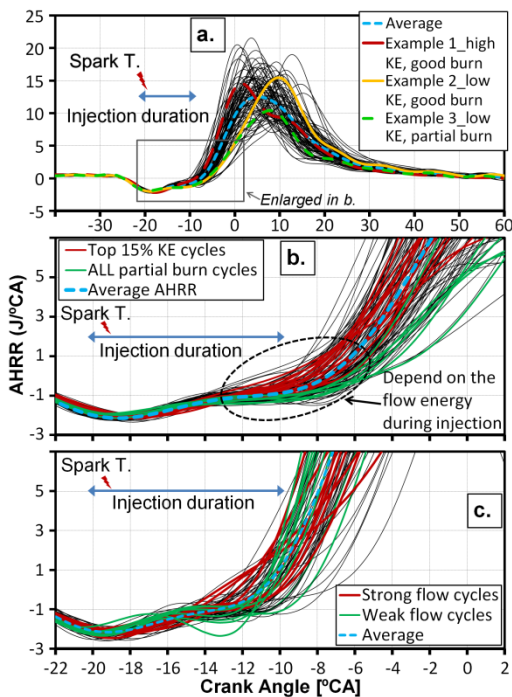

Fig.8. (a) AHRR curves for [O$_2$] = 19%, test 5, highlighting the three examples shown in Figs. 4-7, (b) early AHRR with [O$_2$] = 19%, test 5, highlighting the top-15% KE cycles and all partial-burn cycles, and (c) early AHRR curves with [O$_2$] = 21%, test 4, highlighting all strong- and weak-flow cycles.
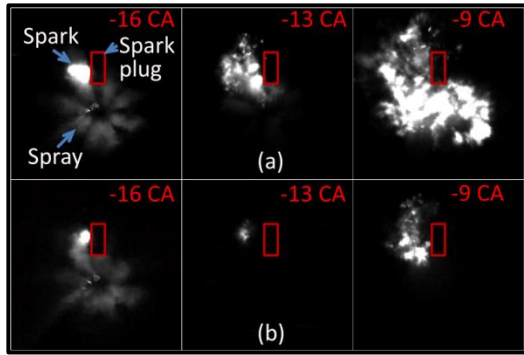
Fig.9. Comparison of early flame propagation for statistically selected cycles from (a) test 4, $[O_2]$ =21%, and (b) test 5, $[O_2]$ =19%. Images at -16°CA include LED illumination of the liquid spray.
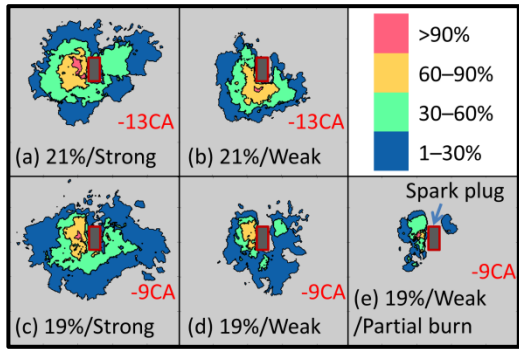

Fig.10. Probability maps of flame development for (a) 10 strong-flow and (b) 10 weak-flow cycles with $[O_2]$ = 21%, (c) 20 strong-flow, (d) 25 weak-flow, and (e) 7 partial-burn cycles with $[O_2]$ = 19%.